31st Annual International Conference of the IEEE EMBS
Minneapolis, Minnesota, USA, September 2-6, 2009

# Macroscopic fluorescent lifetime imaging in turbid media using angular filter arrays

**M. Najiminaini[1], F. Vasefi[1, 2], B. Kaminska[1], G. H. Chapman[1], J. J.L. Carson[2, 3]**

[1]The School of Engineering Science, Simon Fraser University, Burnaby, BC, Canada
[2]Imaging Program, Lawson Health Research Institute, London, ON, Canada
[3]Medical Biophysics, University of Western Ontario, London, ON, Canada

*Abstract*— **We describe an optical imaging methodology applicable to the detection of a fluorescent agent below the surface of turbid media with lifetime property extraction. The method exploits the collimation detection capabilities of an angular filter array to form a projection image of a fluorophore embedded within the tissue-mimicking phantom. A femto-second pulsed laser was used to illuminate the tissue and excite the fluorophore within the medium. Fluorescent emission passing through the angular filter array was detected by an ultra fast gate intensified CCD camera. The array accepted photons with trajectories within 0.5 degree of the axis of each micro-tunnel and rejected most of the scattered fluorescent light exiting the tissue. The performance of the angular filter array did not depend on coherence or wavelength of the laser illumination. It was observed that resulted images had sub-millimeter resolution within 5 mm deep into the turbid media and can have a large field of view (~2 cm x 2 cm).**

## I. Introduction

Fluorescence lifetime imaging is a promising non-invasive imaging modality for the diagnosis of abnormal or malignant tissue. It can provide information about fluorescence intensity, lifetime, and spectral content, which can be used to characterize the chemical composition, metabolism, and environmental factors of tissues and biological samples [1]. In general, tissue remitted fluorescence light intensity is measurable near the tissue surface with techniques such as epifluorescence microscopy [2] and confocal fluorescent microscopy [3]. But recently, researchers have developed methods to extract fluorophore lifetime information from deeper tissues [4]-[8]. Diffuse fluorescence from deep tissues has also been investigated as a tool of tumor detection by tracing the center of fluorescing targets [9]-[11]. This advancement relies on the fact that the suitably designed fluorophore will accumulate in tumors preferentially.

However, photons from fluorescence generation that propagate from deep tissues undergo multiple scattering events and appear to follow a random walk. Furthermore, remitted fluorescence light declines rapidly with depth of fluorescence generation. Therefore, remitted photons produce images with low spatial resolution and poor localization of fluorescent markers located deep in tissue.

In this paper, to overcome the limitations to fluorescent imaging imposed by optical scatter, a micro-machined silicon angular filter array (collimator) was used to filter unwanted remitted fluorescent scattered photons and accept the image forming fluorescent photons based on photon trajectory [12]-[15]. The time resolved fluorescence emitted photons passing through the angular filter array were detected by an ultra fast gate intensified CCD camera. Then, the temporal profile of the reemitted fluorescent signal was recorded and the lifetime parameter was extracted using the Laguerre Deconvolution Technique (LDT).

Angular Domain Fluorescence Imaging

Angular domain fluorescence imaging employs an Angular Filter Array (AFA) to filter unwanted remitted fluorescent scattered photons and pass the informative photons based on acceptance angle [12]-[15]. As shown in Figure 1, the angular filter device differentiates between minimally scattered fluorescent photons from the more plentiful scattered fluorescent photons emitted from fluorophores located in tissue. The scattered photons emitted from fluorophores have less likelihood of exiting the tissue surface with an angular deviation acceptable to the AFA. Only photons emitted from the fluorophore that have small angular deviation are accepted by the AFA. Hence, these minimally deviated photons can pass through the AFA and be detected by the camera. Since the performance of the AFA is not dependent on coherence, or the wavelength of light, angular domain fluorescence imaging can be used to map fluorophores over a large field-of-view with sub-millimeter spatial resolution at significant depth into tissue (~ 5 mm).

Recently, we investigated a new design for the angular filter array, which consisted of a parallel array of square-shaped micro-tunnels 80 microns wide and tall along a 1.5 cm long plate to obtain aspect ratios of approximately 188:1 (see Figure 2). The bottom component of the AFA was fabricated by etching a silicon substrate. The walls of the bottom component were patterned with many small features to suppress internal reflections within each micro-tunnel.

A flat silicon wafer was used as the top component to enclose the micro-tunnels to form the AFA. Because the micro-tunnels were square in geometry, there existed an

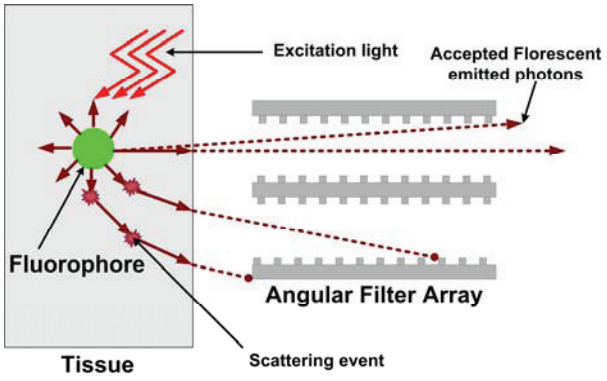


Figure 1. Fluorescence optical imaging principle using an angular filter array.

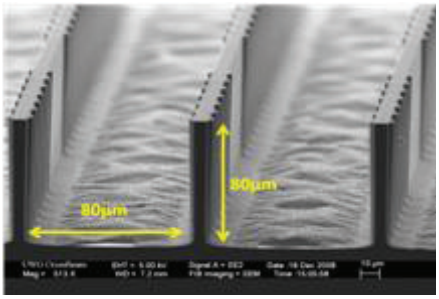


Figure 2. Silicon micro-machined angular filter array (bottom component).

angular acceptance angle variation from 0.3° (wall to wall) to 0.42° (corner to corner). This design was selective enough to collect quasi-ballistic photons that provided at least 200 µm spatial resolution for targets embedded in turbid media.

## II. Methodology

### A. Experimental setup

The experimental setup based on the ADI configuration in the reflection mode is shown in Figure 3. In this mode, both the illumination source and the aligned detector system are located on the same side of the imaged sample. The fluorescent target was excited by light from the pulsed laser source. Fluorescence emission was detected using a gate-intensified CCD camera. Time gating of the camera was synchronized to the pulsed laser source.

A fiber-based pulsed laser was employed for all experiments. It had a pulse width of 100 fs, a repetition rate of 50 MHz, and an average power of 20 mW. The pulsed laser emitted 780 nm and 1560 nm light. The free space beam was collimated and had a diameter of 2.4 mm. The beam was reshaped into a collimated line of light to cover the AFA channel openings. The AFA was aligned precisely at the same height as the light source to enable capture of the in-line fluorescent emission. A Keplerian lens system was located between the sample and the AFA. The lens system transferred fluorescent emission from the sample to the AFA and a dichroic mirror was placed between the lenses of the Keplerian systems to enable laser light delivery. An ultra-fast gate-intensified CCD camera (PicoStar HR, LaVision) was used to detect the light exiting the micro-tunnels. The intensifier employs a voltage-gated micro-channel plate (MCP) controlled by a high rate imager (HRI, Kentech Instruments, UK) and has single-photon detection sensitivity.

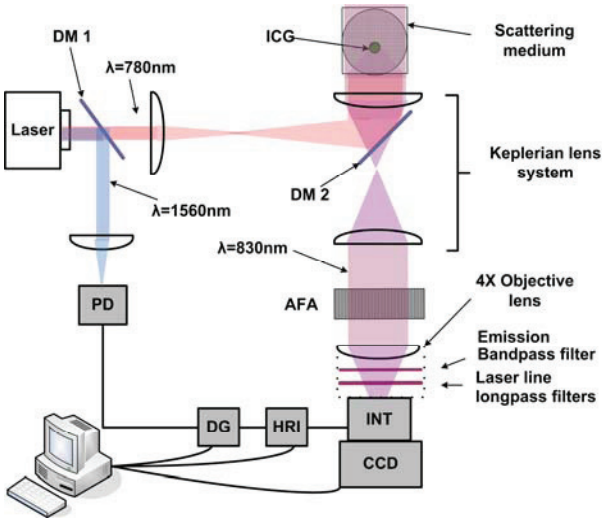


Figure 3. Optical imaging setup. (Abbreviations: CCD, charge-coupled device; HRI, high rate imager; INT, intensifier; DG, delay generator; DM, dichroic mirror; AFA, angular filter array; ICG, indocyanine green; and PD, photo diode)

To gate the intensifier, a pulsed negative voltage across a photocathode was employed in front of the MCP. The gate width was adjustable via an ultra-short pulse generated by the HRI, with nominal gate width settings from 200 to 1000 ps. The output of the intensifier was connected to a 12-bit CCD camera of 1370 by 1040 pixels. The ICCD operated as a very quick shutter and was synchronized with the laser pulses through a delay unit (Delay Unit, LaVision, Germany). After the image intensifier, the CCD camera integrated light over a fixed exposure time below the camera saturation level. With the image intensifier operating in a "comb" mode, a sequence of gated transmissions accumulated on the CCD. The fluorescence emission passing through the scattering medium was spatially filtered by AFA and temporally resolved by scanning the delay time (Td) between the laser pulse and the time-gated detection using image capture and control software (DaVis, LaVision). The system recorded the light coming of all the micro-tunnels of the AFA. The delay was scanned electronically in order to record the temporal point spread function (TPSF) typically in 15-ps steps. The fluorescence photons were spectrally separated from the incident illumination by a short band-pass interference filter (FL830-10, Thorlabs, NJ, USA), and 785nm laser line long-pass filter (NT47-508, Edmund Optics Inc., NJ, USA) prior to reaching the camera. To obtain the reference signal for synchronization between the pulsed laser and the gate-intensified CCD camera, a dichroic mirror was used to reflect the 1560 nm component emitted by the pulsed laser. The deviated beam is focused on to an InGaAs photodiode (ET-3000, Electro-Optics Technology, Inc.). The photodiode output signal was

connected to the sync in port of the delay generator unit.

Samples were prepared using an aqueous suspension of Intralipid™. The scattering behavior of Intralipid™ is similar to tissue at visible and near infrared wavelengths. Moreover, Intralipid™ has low optical absorption in the visible and near infrared region of the spectrum [16]-[18]. To examine the spatial resolution of the system, 1.2 mm diameter clear glass tubes filled with 20 μM indocyanine green (ICG) diluted with water were used. Since the optical properties of water/ICG solution change over time, the ICG samples are prepared on the same day as each experiment. ICG was selected since it can be excited at the same wavelength as the pulsed laser source.

### *B. Fluorescent lifetime extraction*

The time-resolved Fluorescent Impulse Response Function (FIRF), which contains fluorescent lifetime information, was estimated using the Laguerre Deconvolution Technique (LDT) [19]-[20]. The LDT method expands the FIRF on the discrete time Laguerre basis. The Laguerre Functions (LFs) consist of an orthonormal basis with exponential expressions. They are considered a suitable model for physical systems with asymptotically exponential relaxation dynamics.

The measured fluorescence intensity decay data *y(n)* was considered as the discrete convolution of the FIRF *h(n)* with the system response *x(n)*:

$$y(n) = T.\sum_{m=0}^{K-1} h(m)x(n-m), \quad n = 0, \dots, K-1, \tag{1}$$

where $K$ is the number of data samples, and $T$ is the sampling interval. The orthonormal set of discrete time LFs $b_j^{\propto}(n)$ is used to expand *h(n)*:

$$h(n) = \sum_{j=0}^{L-1} c_j b_j^{\propto}(n), \tag{2}$$

where $c_j$ are the unknown Laguerre Expansion Coefficients (LEC), $b_j^{\propto}(n)$ is the *j'*th order orthonormal discrete LF, and L is the number of LFs used to expand the FIRF. The LF basis is:

$$b_j^{\propto}(n) = \propto^{\frac{n-j}{2}} (1-\propto)^{\frac{1}{2}} \sum_{k=0}^{j} (-1)^k \binom{n}{k}\binom{j}{k} \propto^{j-k} (1-\propto)^k, \quad n \geq 0, \tag{3}$$

where α parameter ($0 < \alpha < 1$) specifies the rate of exponential decay of the LF. Hence, acquiring a higher α parameter represents a FIRF with a larger lifetime. By inserting equation (2) to (1) , the *y(n)* becomes:

$$\begin{aligned} y(n) &= \sum_{j=0}^{L-1} c_j\, v_j(n), \\ v_j(n) &= T \sum_{m=0}^{K-1} b_j^{\propto}(m)x(n-m). \end{aligned} \tag{4}$$

where $v_j(n)$ are the discrete time convolutions of the system response *x(n)* with the LF of order *j*. The unknown coefficients are estimated by using the generalized linear least-square solution of equation (4):

$$min \left| \sum_{j=0}^{L-1} c_j v_j(n) - y(n) \right|^2 \tag{5}$$

The number of Laguerre functions (L) and the α-value was determined by minimizing the normalized mean square error (NMSE) and examining the residuals for randomness. Fitting was performed for values of L between 1 and 6 and α between 0.6 and 0.9. Each combination of these parameters in LTD were applied to the measured data to find optimal values for L and α. Optimal values for L and α of 4 and 0.88 were determined, respectively.

## III. Results and Discussions

The angular domain fluorescent imaging system was able to image time-resolved fluorescent signals over a large two-dimensional area of the sample with sub-millimeter resolution. Sub-millimeter spatial resolution was possible due to the use of an AFA with sub-millimeter channel openings. The AFA covered a long line-shaped field of view, which permitted two-dimensional images to be captured by scanning the sample with the AFA and stacking the line images into a 2-dimensional image.

The spatial map of the fluorescent targets (two glass tubes each filled with 20 μM ICG) in scattering medium is shown in Figure 4. The fluorescent targets were placed 5 mm deep into a 5 cm optical cuvette. The glass tubes had 1 mm internal diameter and 1.2 mm outer diameter. The two tubes were located 4 mm apart. The fluorescence emission was captured with the ultra fast gate-intensified CCD camera with 1000 ps temporal gate width, which captured the first 1000 ps of fluorescence emission due to each laser pulse (i.e. quasi-ballistic plus scattered photons). Figure 4 shows the scanned image and the average light intensity as a function of position along the AFA. Image contrast was 3:1.

Temporal scans of fluorescent emission from ICG are shown in Figure 5. For each scan a 150 fs laser pulse was used to illuminate the sample and the fluorescent emission at a variety of time points using a 15 ps step size was recorded with the ultra fast gate-intensified CCD camera coupled to an angular filter. The instrument response was determined by recording the temporal response of the system to the laser pulse that passed through the same optical path, but was reflected at the sample position by a mirror. The fluorescence impulse response was then derived by deconvolution of the temporal scan of the fluorescence emission by the instrument response. Photo-bleaching was also apparent in the scan, which degraded the signal intensity over time (apparent as a decrease in signal from bottom to top in the image). Other fluorescent dyes with better immunity to photo-bleaching and higher quantum yield would be more desirable to improve the number of captured fluorescent photons. In these experiments, the integration time for each line of the scan was 160 ms and could be extended to improve the signal to noise in the

images. For example, the integration time could have been extended to up to 2 s with only a 50% increase in acquisition time, since up to 2 seconds was associated with the overhead of the communication between the stage controller and other electronics.

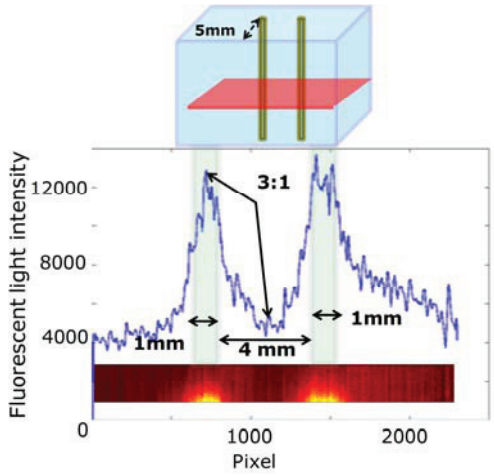


Figure 4. Angular domain fluorescent imaging in turbid media. Targets were two glass tubes filled with 20 µM ICG diluted in water and placed in 5 mm deep inside a cuvette filled with 0.1% Intralipid. ($\mu_s'$ = 0.8 cm$^{-1}$ , $\mu_a$ = 0.01 cm$^{-1}$).

Figure 6 (a)-(c) shows the normalized FIRF for different camera temporal gate widths corresponding to the data shown in figure 5(a)-(c), respectively. The resultant graphs were normalized by the following equation:

$$NFIRF(n) = \frac{FIRF(n) - \min\big(FIRF(n)\big)}{\max\big(FIRF(n)\big) - \min\big(FIRF(n)\big)}. \quad (6)$$

Two model functions of the fluorescence decay were used to fit each NFIRF and obtain estimates of the average fluorescence lifetime. The first function was a single exponential decay model,

$$I(t) = I_0 e^{\frac{-t}{\tau_{avg}}}. \quad (7)$$

where $\tau_{avg}$ represents the average fluorescence lifetime. The second function was a bi-exponential decay model,

$$I(t) = A_1 f_M e^{\frac{-t}{\tau_1}} + A_1 f_T e^{\frac{-t}{\tau_2}} \quad (8)$$

where $\tau_1$ and $\tau_2$ represent the time constants, $A_1$ represents the relative amplitude ($A_1$), and $f_M$ and $f_T$ represent the fractional steady-state intensity of each component ($f_M$ + $f_T$=*1*) [21], [22]. As shown in Figure 6, the bi-exponential function fit each NFIRF with higher correlation than the single exponential function. From these fits we estimated the average fluorescence lifetime from the single exponential model directly and the bi-exponential model using the fractional steady-state intensities ($f_M$ and $f_T$) as follows:

$$\tau_{avg} = f_M \tau_1 + f_T \tau_2.$$

The numerical values of parameters for the fitted curves are shown in Table 1.

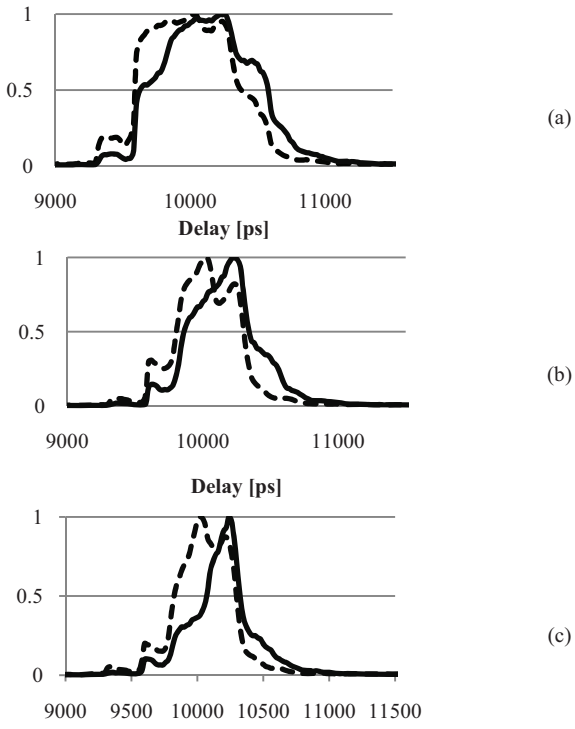


Figure 5. Temporal scan of ICG fluorescence decay (normalized) (solid line) versus the instrument response from a 150 fs laser pulse (dash line) that travelled the same optical path versus temporal delay (ps). Camera temporal gate width of (a) 1000 ps, (b) 500 ps, and (c) 200 ps.

One possible reason for the lack of a good mono-exponential fit on the deconvolved NFIRF function may due to ICG photobleaching. This can be due to the immobilized fluorophore samples placed inside the Intralipid solution.

TABLE I
NUMERICAL VALUES OF THE NFIRF CURVE FITTING

| Temporal gate width | Conversion from Gaussian and CGS EMU to SI [a] |
|---|---|
| Single exponential fitting (1000 ps) | $h(n) = 0.496e^{-\frac{n}{514\times10^{-12}}}$ |
| Double exponential fitting (1000 ps) | $h(n) = 1.037e^{-\frac{n}{147\times10^{-12}}} + 0.007e^{-\frac{n}{505\times10^{-10}}}$ |
| Single exponential fitting (500 ps) | $h(n) = 0.575e^{-\frac{n}{500\times10^{-12}}}$ |
| Double exponential fitting (500 ps) | $h(n) = 0.890e^{-\frac{n}{188\times10^{-12}}} + 0.002e^{-\frac{n}{946\times10^{-10}}}$ |
| Single exponential fitting (200 ps) | $h(n) = 0.434e^{-\frac{n}{577\times10^{-12}}}$ |
| Double exponential fitting (200 ps) | $h(n) = 0.961e^{-\frac{n}{167\times10^{-12}}} + 0.005e^{-\frac{n}{630\times10^{-12}}}$ |

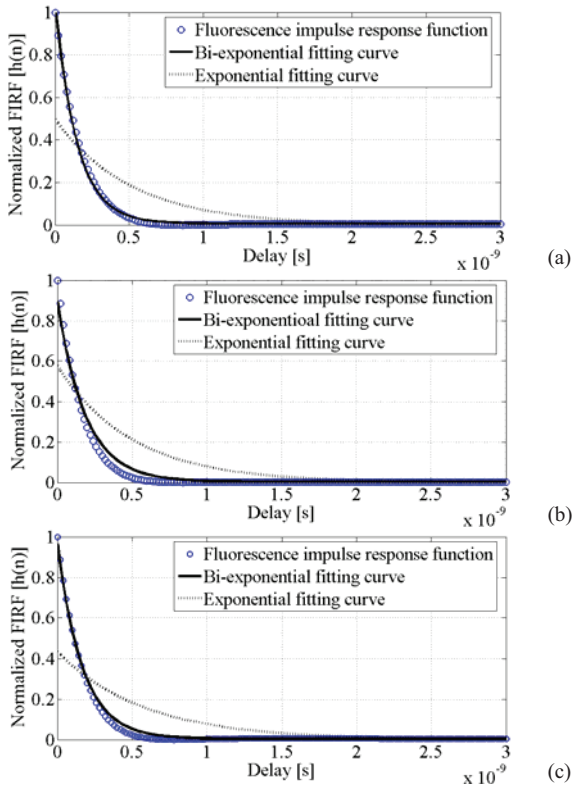


Figure 6. Fluorescence intensity decay computed from data collected with a temporal gate width of (a) 1000 ps, (b) 500 ps, and (c) 200 ps.

## IV. Conclusion

This paper presents a fluorescent imaging system based on ADI that can detect fluorescent targets deep (~ 5 mm) within a turbid medium. Fluorescent line targets <1 mm in diameter could be resolved. The informative fluorescent photons that travelled straight trajectories exited the turbid medium with small angular deviation. These minimally deviated photons could be distinguished by inserting an angular filter array with a small acceptance angle into the optical path before the detector. The time-resolved measurements using the pulsed laser, the AFA, and an ultra fast gate-intensified CCD camera demonstrated that fluorescence lifetime imaging using the ADI methodology was feasible. The lifetime parameter can be extracted by fitting to the bi-exponential curve and calculating the average decay value.

## Acknowledgment

This project was funded by grants from the Natural Sciences and Engineering Research Council of Canada (NSERC) to Bozena Kaminska and Dr. Jeffery J.L. Carson. In addition, partial funding was provided by a Translational Breast Cancer Studentship to Fartash Vasefi from the London Regional Cancer Program.

## References

[1] S. B. Bambot, J. R. Lakowicz, G. Rao, "Potential applications of lifetime-based, phase-modulation fluorimetry in bioprocess and clinical monitoring," *Trends in Biotechnology 13*, pp. 106-115, 1995.

[2] D. W. Piston, M. S. Kirby, H. Cheng, W. J. Lederer, and W. W. Webb, "Two-photon-excitation fluorescence imaging of three-dimensional calcium-ion activity," *Appl. Opt. 33*, pp. 662-669, 1994.

[3] Diaspro, "Confocal and Two-Photon Microscopy: Foundations, Applications and Advances," *Wiley-VCH*, New York, pp. 101-125, 2001.

[4] E. M. Sevick-Muraca and C. L. Burch, "Origin of phosphorescence signals reemitted from tissues," *Opt. Lett. 19*, pp. 1928-1931, 1994.

[5] M. S. Patterson and B. W. Pogue, "Mathematical model for time-resolved and frequency-domain fluorescence spectroscopy in biological tissues," *Appl. Opt. 33*, pp. 1963-1974, 1994.

[6] J. Tromberg, S. Madsen, C. Chapman, L. O. Svaasand, and R. C. Haskell, "Frequency-domain photon migration in turbid media," in *Advances in Optical Imaging and Photon Migration OSA Proceedings*, vol. 21, pp. 93-95, 1994.

[7] J. Durkin, S. Jaikumar, N. Ramanujam, and R. Richards-Kortum, "Relation between fluorescence spectra of dilute and turbid samples," *Appl. Opt. 33*, pp. 414-423, 1994.

[8] J. Wu, M. S. Feld, and R. P. Rava, "Analytical model for extracting intrinsic fluorescence in turbid media," *Appl. Opt. 32*, pp. 3585-3595, 1993.

[9] Knuttel, J. M. Schmitt, R. Barnes, and J. R. Knutson, "Acousto-optic scanning and interfering photon density waves for precise localization of an absorbing (or fluorescent) body in a turbid medium," *Rev. Sci. Instrum*, vol. 64, pp. 638-644, Mar. 1993.

[10] M. A. O'Leary, D. A. Boas, B. Chance, and A. G. Yodh, "Reradiation and imaging of diffuse photon density waves using fluorescent inhomogeneities," *Journal of Lumin. 60-61*, pp. 281-286, 1994.

[11] Wu, Y. Wang, L. Perelman, I. Itzkan, R. R. Dasari, and M. S. Feld, "Time-resolved multichannel imaging of fluorescent objects embedded in turbid media," *Opt. Lett. 20*, pp. 489-491, 1995.

[12] G. H. Chapman, "Angular domain imaging of objects within highly scattering media using silicon micromachined collimating arrays," *Selected Topics in Quantum Electronics, IEEE Journal on,* vol. 9, pp. 257, 2003.

[13] F. Vasefi, "Multi-spectral angular domain optical imaging in biological tissues using diode laser sources," *Optics Express,* vol. 16, pp. 14456, 2008.

[14] F. Vasefi, "Image contrast enhancement in angular domain optical imaging of turbid media," *Optics Express,* vol. 16, pp. 21492, 2008.

[15] F. Vasefi, "An Optical Imaging Technique Using Deep Illumination in the Angular Domain," *Selected Topics in Quantum Electronics, IEEE Journal on,* vol. 13, pp. 1610, 2007.

[16] Optical properties of "Intralipid™", an aqueous suspension of lipid droplets [Online]. Available: http://omlc.ogi.edu/spectra/intralipid/

[17] index.html.

[18] H. V. Staveren, C. Moes, J. Van Marle, S. Prahl, and M. V. Gemert, "Light scattering in Intralipid-10% in the wavelength range of 400-1100 nanometers," *Appl. Opt. 30*, pp. 4507-4514, 1991.

[19] J. A. Jo, Q. Fang, T. Papaioannou, J. D. Baker, A. H. Dorafshar, T. Reil, J.H. Qiao, M. C. Fishbein, J. A. Freischlag, and L. Marcu, "Laguerre-based method for analysis of time-resolved fluorescence data: application to in-vivo characterization and diagnosis of atherosclerotic lesions," *Journal of Biomedical Optics*, vol. 11, pp. 021004-1-021004-13, April 2006.

[20] J. A. Jo Q. Fang T. Papaioannou, and L. MarcuFast, "Model-free deconvolution of fluorescence decay foranalysis of biological systems," *Journal of Biomedical Optics*, vol. 9, no.4, pp. 743-752, Aug. 2004.

[21] E. Kuwana and E. M. Sevick-Muraca, "Fluorescence Lifetime Spectroscopy in Multiply Scattering Media with Dyes Exhibiting Multiexponential Decay Kinetics," Biophysical Journal, vol. 83, pp. 1165-1176, Aug. 2002.

[22] J. R. Lakowicz, "Principles of Fluorescence Spectroscopy," 3rd Ed., chapter 4, Springer US, New York, 2006.